Numerical and Experimental Study of the Front Surface Recombination Velocities and Base Widths Effect in Multi-Crystalline Silicon Solar Cell Quantum Efficiency

Bilel Abdouli, Lotfi Khezami, Ahlem Guesmi, Aymen Amine Assadi, Mohamed Ben Rabha

crystals

MDPI

Article

Numerical and Experimental Study of the Front Surface Recombination Velocities and Base Widths Effect in Multi-Crystalline Silicon Solar Cell Quantum Efficiency

Bilel Abdouli [1], Lotfi Khezami [2], Ahlem Guesmi [2], Aymen Amine Assadi [3] and Mohamed Ben Rabha [1,*]

[1] Laboratoire de Nanomatériaux et Systèmes pour Énergies Renouvelables, Centre de Recherches et des Technologies de l'Énergie, Technopôle de Borj-Cédria, BP 95 Hammam-Lif, Tunis 2050, Tunisia
[2] Department of Chemistry, Imam Mohammad Ibn Saud Islamic University (IMSIU), P.O. Box 5701, Riyadh 11432, Saudi Arabia
[3] École Nationale Supérieure de Chimie de Rennes, ENSCR, Université de Rennes, 11 Allée de Beaulieu, 35708 Rennes, France
* Correspondence: rabha22222@yahoo.fr

Abstract: Photovoltaic research activities are related to material innovation that can be obtained at a comparatively low cost. Semiconductor p-type multi-crystalline Czochralskyc (CZ)-grown silicon wafers were used in this study. The effects of front surface recombination velocities and base thickness in solar cells' quantum efficiency are theoretically calculated. The results denote that both the surface recombination velocities and the base widths significantly impact the quantum efficiency. The results are of universal technical importance in designing solar cells and their surface structures. The main goal of this paper was to confirm the validity of the above theoretical calculations; for this purpose, silicon solar cells with front-thin porous silicon and rear interdigitated contact have been produced. A good agreement was obtained between experimentally obtained solar cells' quantum efficiency data and the theoretical results. Therefore, the quantum efficiency of the mc-Si solar cells with porous silicon and rear interdigitated contact was enhanced up to 25% at 580–1100 nm wavelength range and up to 50% at short wavelength (400–570 nm), compared to reference mc-Si solar cells. The obtained results indicate that the rear interdigitated contact maximizes the surface area of the metal contact and improves the current collection. At the same time, the porous silicon layer passivates the front surface and reduces recombination losses.

Keywords: semiconductors; silicon; solar cells; porous silicon; interdigitated contact; quantum efficiency

Citation: Abdouli, B.; Khezami, L.; Guesmi, A.; Assadi, A.A.; Rabha, M.B. Numerical and Experimental Study of the Front Surface Recombination Velocities and Base Widths Effect in Multi-Crystalline Silicon Solar Cell Quantum Efficiency. *Crystals* **2023**, *13*, 425. https://doi.org/10.3390/cryst13030425

Academic Editors: Nicolò Lago, Mirko Seri and Andrea Cester

Received: 29 January 2023
Revised: 23 February 2023
Accepted: 27 February 2023
Published: 1 March 2023

1. Introduction

The research activities on silicon solar cells are related to the material development that can be achieved at low cost, focusing on improving the conversion efficiency of multi-crystalline silicon (mc-Si), which is a very attractive material for solar cell processing due to its low wafer cost compared to crystalline silicon.

Notably, the specific doping levels for n-type and p-type regions in n-p homo-junction multi-crystalline silicon solar cells consisting of a single type of semiconductor material are 10^{16} and 10^{18} cm^{-3}, respectively. The p-type serves as the base of the solar cell of a few hundred microns' thickness, while the n-type region is typically used as the front region having a thickness of a few microns, as it facilitates the efficient collection of photo-generated carriers [1]. Thicker p-type regions can increase light absorption and carrier lifetime but also increase recombination losses and reduce efficiency [2]. The fabrication of PN devices such as PIN and how to investigate the doping level or geometrical parameters were obtained [3,4].

On the other hand, the photo-generated current strongly relates to the solar cells' quantum efficiency. One has to raise the solar cells' quantum efficiency to enhance conversion

efficiency. The front-thin porous silicon layer serves to reduce the surface recombination velocities (Sf) and reduce the reflectivity of the cell, thereby increasing the amount of incident light absorbed by the active region of the cell [5]. Furthermore, thick silicon solar cells suffer from unavoidable losses in power conversion efficiency due to the non-radiative recombination of photo-generated charge carriers during their relatively long path to electrical contacts at the extremities of the cell. It means that varying the base width affects the bulk recombination and the collection probability of the photo-generated charge carriers. Based on this fact, the structure's electrical and optical performance will change. In addition, the grooving structure is designed to maximize the surface area of the contact with the metal electrodes, reducing the series resistance and improve the current collection, leading to higher efficiency. Silicon grooves can be created using a variety of techniques. The choice of technique depends on the specific application and the desired groove characteristics, such as aspect ratio, depth, and width. The most common techniques are the wet electrochemical [6,7], mechanical grooving [8,9], and laser [10,11] used to create very precise grooves but these are slower than other techniques and require refining or polishing.

Combining the front-thin porous silicon layer and rear interdigitated contact structure in a silicon solar cell can have several benefits. The porous silicon layer improves light trapping, passivates the front surface, and reduces recombination losses at the front [12–14], where the interdigitated contact structure is designed to maximize the surface area of the contact with the metal electrodes and improve the current collection [15], leading to higher efficiency. Applications for this type of silicon solar cell include various kinds of solar energy systems.

This work was developed in two parts. The first part was dedicated to the theoretical calculation of the effect of front surface recombination velocities (Sf) and base thickness (Hb) in solar cells' quantum efficiency of p–n homo-junction silicon solar cells. Hence the second part was dedicated to confirming the validity of the theoretical calculations with experiment one. For this purpose, silicon solar cells with front-thin porous silicon and rear interdigitated contact were systematically investigated and compared with reference multi-crystalline silicon solar to explain the effect of this treatment on photovoltaic performances. Scanning electron microscope, Fourier-transform infrared spectroscopy, and quantum efficiency were performed to investigate the manufactured multi-crystalline silicon solar cells.

2. Theoretical Calculation of S_f and H_b Effect in Solar Cell Quantum Efficiency

Next, we calculate the separate regions of a flat silicon solar cell donations in the quantum efficiency based on the structure where the sketch and the schematic of n-p homo-junction solar cell were separately shown in Figure 1a,b. Yang et al. [16] are also investigating the effect of the size structure of the cell on the solar cell's quantum efficiency. The front (emitter) contribution of the QE is given by [17–19]:

$$QE_{Fron}(\lambda) = \frac{\alpha L_f}{(\alpha^2 {l_f}^2 - 1)} \left[\alpha L_f \exp(\alpha x_j) + \frac{(\frac{S_f L_f}{D_f} + \alpha L_f) \exp(\alpha x_j)(\frac{S_f L_f}{D_f}) ch(\frac{x_j}{L_f}) + sh(\frac{x_j}{L_f}))}{(\frac{S_f L_f}{D_f}) sh(\frac{x_j}{L_f}) + ch(\frac{x_j}{L_f})} \right] \quad (1)$$

where: λ, α, L_f, S_f, and D_f denote the wavelength of sunlight, the absorption coefficient, the diffusion lengths, the surface recombination velocity, and the diffusion coefficient of the front (emitter), respectively.

The base impact was obtained by Y. Kuo-Hui, Y. Jaw-Yen [16], and M. Wolf, M.B. Prince [19]. The calculations of the solar cells' quantum efficiency in the base region were first given by the following equation [20]:

$$QE_{Base}(\lambda) = \frac{\alpha L_b \exp(-\alpha A)}{(\alpha^2 {l_b}^2 - 1)} \left[\alpha L_b - \frac{(\frac{S_b L_b}{D_b}) ch(B) - \exp(-\alpha C) - sh(B) + \alpha L_b \exp(\alpha C)}{(\frac{S_b L_b}{D_b}) ch(B) + sh(B)} \right] \quad (2)$$

where: L_b is the base diffusion lengths; D_b is the diffusion coefficient of the base; S_b is the back recombination velocity.

$$A = X_j + W; B = \frac{(H_b - X_j - W)}{L_b} \text{ and } C = H_b - X_J - W$$

Related to the above process, the influence of the space-charge region to the solar cells' quantum efficiency is given by following expression:

$$QE_{Scr}(\lambda) = \exp(-\alpha x_j)[1 - \exp(-\alpha w)] \quad (3)$$

The total QE is the sum of the contributions of the separate parts and is given by the resulting formula:

$$QE(\lambda) = QE_{Front}(\lambda) + QE_{Base}(\lambda) + QE_{scr}(\lambda)$$

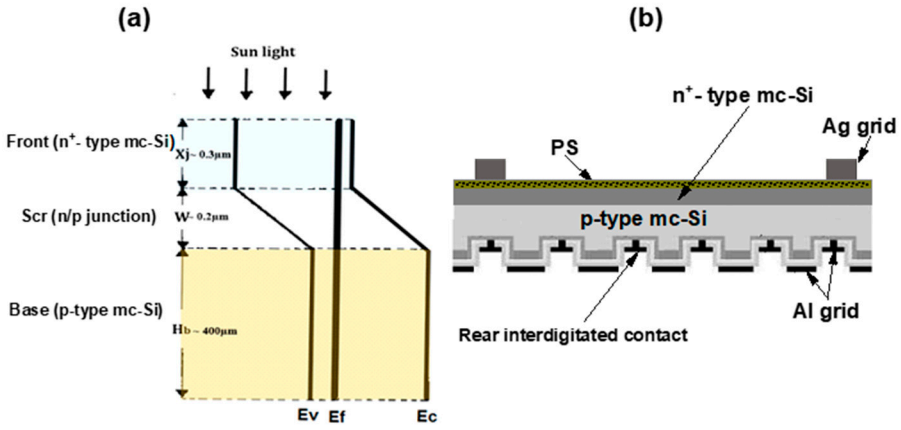

Figure 1. (**a**) Sketch and (**b**) schematic of n-p homo-junction solar cell (Xj, W, and H_b represent the thicknesses of the front, space-charge, and base regions, respectively).

To study the impact of the base width on the separate parts of the solar cells' quantum efficiency, we consider a cell structure with fixed electrical cell parameters and vary only the base widths (400, 300, and 200 µm). For the following discussion the cell parameters from Table 1 are considered to calculate the solar cells' quantum efficiency in the different regions.

Table 1. Fixed electrical cell parameters used theoretical calculation of front surface recombination velocities and base thickness in solar cells quantum efficiency.

Region	Diffusion Coefficient (cm^2/s)	Diffusion Lengths (µm)	Recombination Velocity (cm/s)
Front	$D_f = 6$	$L_f = 10$	$S_f = 0.5*E^4$
Base	$D_b = 20$	$L_b = 100$	$S_b = 1*E^8$

As shown in Figure 2a for different base widths, different quantum efficiency results can be seen. Once the base width rises, the contribution of the base to the quantum efficiency also increases, meaning that the quantum efficiency is a function of the base width. However, the contributions of the emitter (front) and space-charge region are practically unchanged. The variation of the base thickness (400, 300, and 200 µm) affects the quantum efficiency in the wavelength ranging from 530 to 1100 nm. The total quantum efficiency can be enhanced up to 20% at this wavelength, as shown in Figure 2a. The quantum efficiency versus the front surface recombination velocities S_f is presented in Figure 2b. One can notice the contribution of the front surface recombination velocities

S_f to the silicon solar cell quantum efficiency drops significantly in the short wavelength range [400–530 nm] when the S_f rises, while not influenced by the quantum efficiency of the base and Scr. Therefore, the total silicon solar cell quantum efficiency decreases with increasing S_f in wavelength interval [530, 1100 nm].

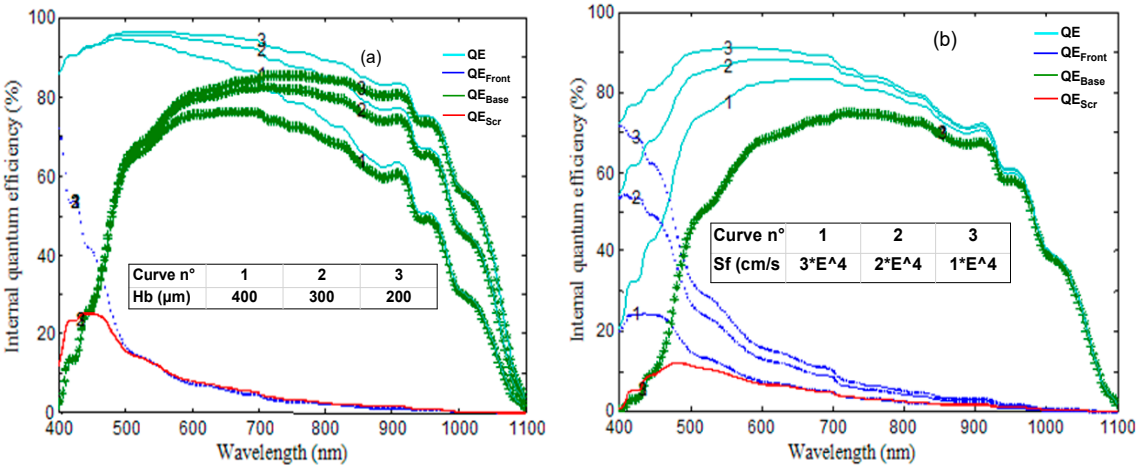

Figure 2. (**a**) Base width and (**b**) front surface recombination effects in the multi-crystalline silicon solar cell quantum efficiency.

3. Experimental Procedure

In this study, industrial p-type mc-Si Czochralskyc (CZ)-grown crystalline wafers having a thickness of about 400 µm, an effective area of 4 cm^2 and a resistivity in the range of 0.5–2.0 Ω cm, were used. A simple, effective, and developed vapor etching process was employed to perform rear silicon grooves and thin porous silicon. The vapor etching practice is achieved in a Teflon Cell located in a special hood taking a filter exhaust fan system seen in Figure 3.

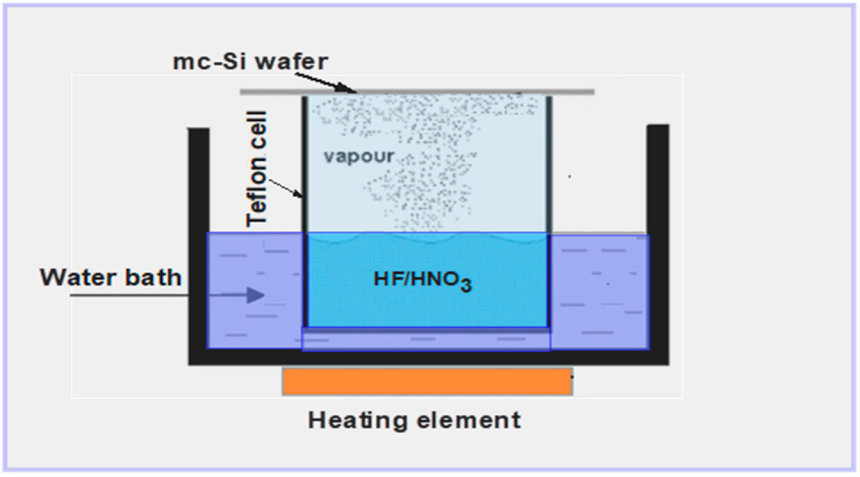

Figure 3. Experimental set-up for the vapor etching technique.

In reality, at volume proportion higher than $\frac{1}{4}$ of HNO_3 (65%) and HF (40%), the CVE performance leads to the $(NH_4)_2SiF_6$ powder formation [21,22], the powder dissolved in H_2O solution leaving grooved areas in the silicon wafer afterward. On the other hand, at a volume proportion lower than $\frac{1}{4}$ of HNO_3 (65%) and HF (40%), the CVE method leads to the realization of thin porous silicon [23,24]. In this investigation, the volume proportion of HNO_3 and HF were fixed to $\frac{1}{2}$ and 1/7 to achieve grooves and porous silicon, respectively, seen in Figure 4a,b. In both cases, the solution of HNO_3 and HF and the silicon wafer temperatures were fixed at 25 and 45 °C, respectively. This temperature modification is

necessary to evade the vapor condensation on the silicon surface in the vapor etching process. After forming the grooves on the Si wafer, the phosphorus diffusion process was achieved to realize the n-p junction at 920 °C. In this case, the average sheet resistance was 25–35 Ω cm, indicating the formation of a relatively homogeneous N+ layer. Front and rear contacts were performed by screen printing a silver paste and an aluminum/silver paste, respectively. After achieving the rear interdigitated contact, a thin PS layer was formed on the front surface of the mc-Si solar cell. There are several reasons why this design may be more stable than other types of solar cells. First, the porous silicon layer is known to be relatively stable over time and is not prone to degradation or other forms of damage. These characteristics means that the cell's performance is less likely to degrade over time due to changes in the properties of the porous silicon layer. Second, the rear interdigitated contact design allows for more efficient charge carrier extraction, which can help reduce the likelihood of charge carrier recombination or other loss mechanisms that can degrade the cell's performance over time. These cells may be well-suited for large-scale deployment in a variety of applications.

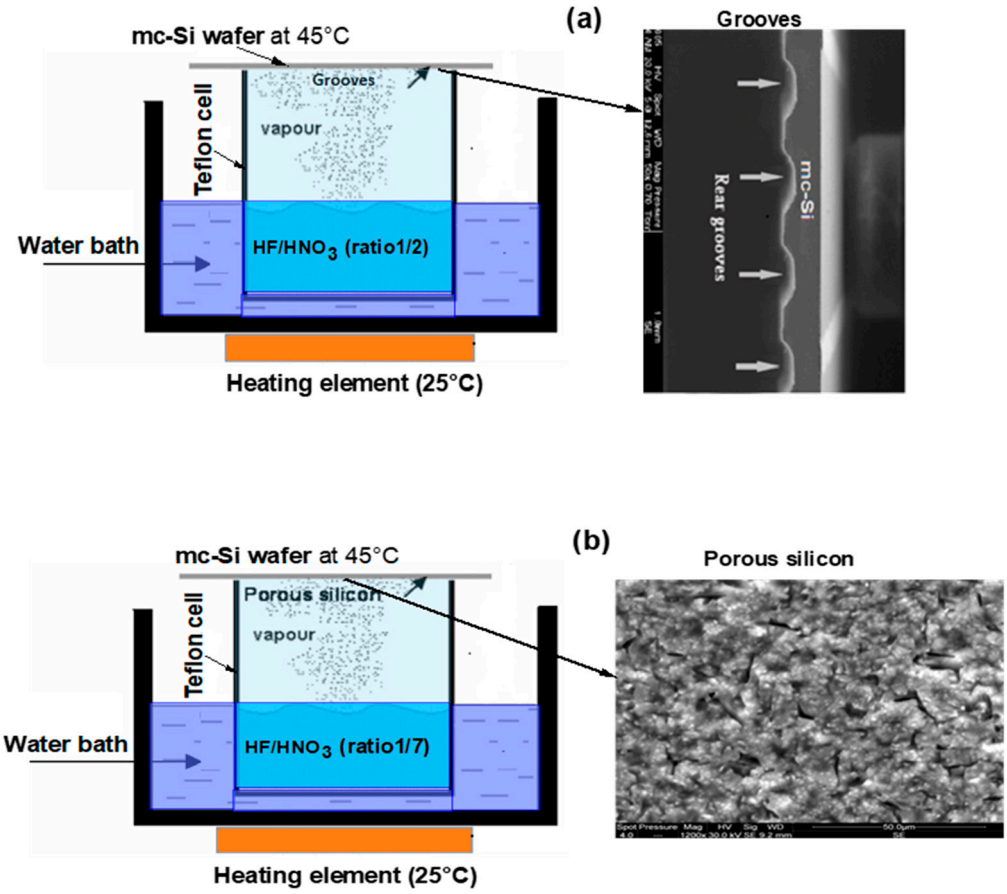

Figure 4. Experimental set-up for the vapor etching technique (**a**) to achieve grooves and (**b**) to achieve porous silicon.

The SEM cross-section view of an mc-Si wafer grooved on the rear region is shown in Figure 4. Figure 4a proves that the grooves' spacing and width were produced apart from the grain orientation of the mc-Si wafer. Moreover, the vapor etching-based grooving method does not require silicon washing as is the case for other methods, such as mechanical processing [25].

4. Results and Discussion

Thick silicon solar cells suffer from unavoidable losses in quantum efficiency due to the non-radiative recombination of photo-generated charge carriers during their relatively

long path to electrical contacts at the extremities of the cell. It means that varying the base width affects the bulk recombination and the collection probability of the photo-generated charge carriers. Based on this fact, the structure's electrical and optical performance will change. The first point is interesting to investigate the effect of rear interdigitated contact on the mc-Si solar cells quantum efficiency, especially in the long wavelength range (base region). Figure 5a illustrates mc-Si solar cells' quantum efficiency for a reference cell with a width base of 400 µm compared to mc-Si solar cells having a width base of 300 and 200 µm. It can be observed that the achievement of rear-buried metallic contacts affects the mc-Si solar cells' quantum efficiency in the 530 to 1100 nm wavelength range by reducing the effective thickness of the base, leading to an increase in the collection probability of the minority carrier at long wavelengths (580–1100 nm spectral range), and then to an enhancement of the mc-Si solar cells quantum efficiency in this spectral region. As a results, the mc-Si solar cells' quantum efficiency can be enhanced up to 25% at the 530–1100 nm wavelength range. The rear interdigitated contact design allows for more efficient charge carrier extraction by providing a large surface area for contact and reducing the distance traveled by the charge carriers to reach the contacts. In summary, the base width is an essential parameter in the design and optimization of silicon solar cells, and it significantly impacts the cells' performance and quantum efficiency. A thinner base width generally leads to higher efficiency and better performance.

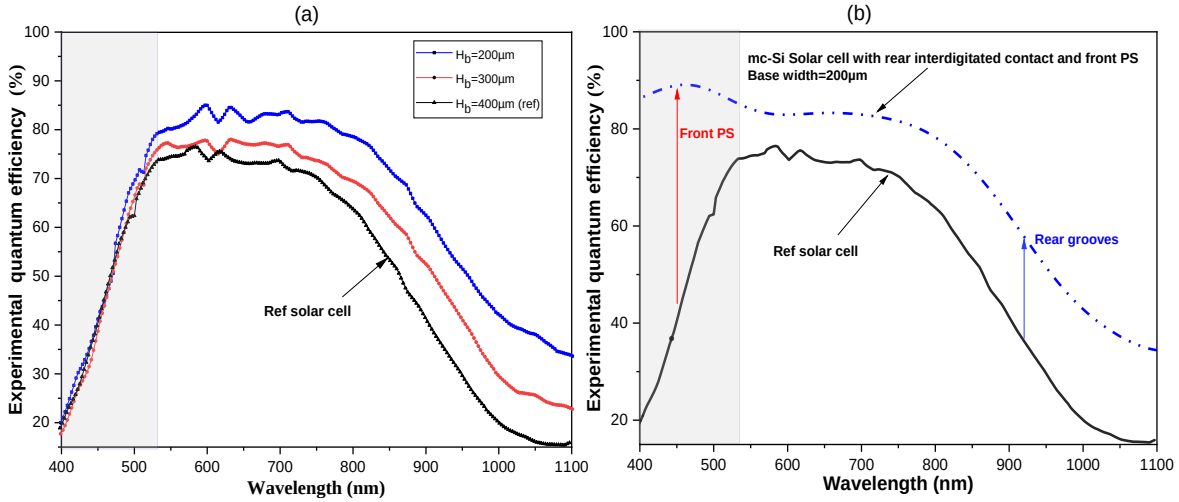

Figure 5. Experimental quantum efficiency of mc-Si solar cells (**a**) with rear interdigitated contact (**b**) with PS/rear interdigitated contact combination compared to ref mc-Si solar cell.

Using a front-thin porous silicon layer on a silicon solar cell can have several benefits, including improved light trapping, passivating the front surface, and reducing recombination losses on the front side of the silicon cell. Additionally, as can be seen in Figure 5b, the application of a thin PS layer by vapor etching method in the front surface of the mc-Si solar cells enhanced the quantum efficiency at a short wavelength range (400–530 nm), where this improvement could be due to the surface recombination velocity diminution via the hydrogen-rich PS layer (Figure 6a) front surface passivation [26–29] and validated by the presence of Si-H bands in the PS layer showed in Figure 6b. Consequently, the quantum efficiency of the mc-Si solar cells was enhanced by over 50% at a short wavelength range compared to mc-Si solar cells without PS. Moreover, the front-thin porous silicon layer serves to reduce the reflectivity of the cell, thereby increasing the amount of incident light that is absorbed by the active region of the silicon solar cell [30]; where observed in Figure 7, the surface reflectance decreased from 29% for the reference device to around 9% for the developed device.

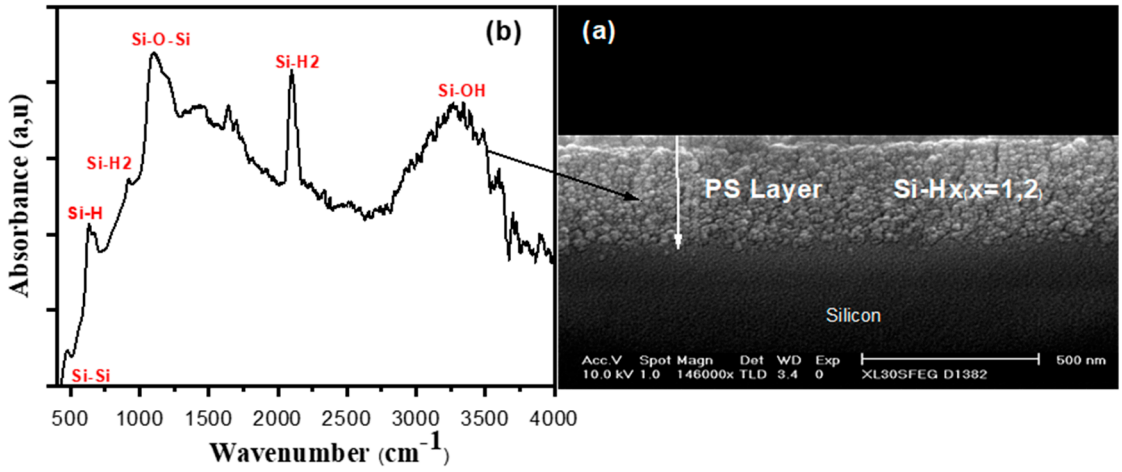

Figure 6. (**a**) SEM surface view of mc-Si after PS formation, (**b**) FTIR spectra of PS.

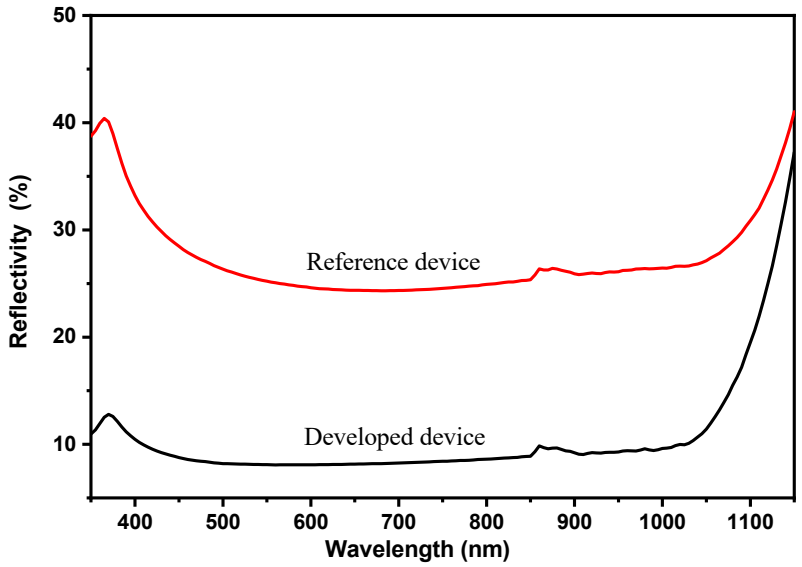

Figure 7. Total reflectivity of mc- Si: for reference and developed device.

In summary, one may notice that to improve a solar cell's spectral response and overall quantum efficiency, decreases in front surface recombination velocities and a base thickness of the silicon solar cell are needed, e.g., by front-thin porous silicon and rear interdigitated contact [31]. To conclude, the combination of front-thin porous silicon and rear interdigitated contact-based mc-Si solar cell design is relatively simple and easy to manufacture, which means that the cells can be produced in large quantities and at a relatively low cost. This finding can help to ensure that the cells are more widely adopted and can be deployed on a larger scale, which can, in turn, helps to improve their stability by reducing the likelihood of manufacturing defects or other issues. Finally, the newly developed devices of front-thin porous silicon and rear interdigitated contact-based mc-Si solar cell generally leads to higher quantum efficiency and better reflectance compared to the reference one (see Table 2). Using porous silicon and rear interdigitated contact-based mc-Si solar cell structures could more efficiently, and cost-effective exploit solar energy. However, challenges remain to be addressed, such as improving the stability and durability of porous silicon and optimizing the rear interdigitated contact-based mc-Si solar cell structure for maximum efficiency.

Table 2. The characteristics of the newly developed devices compared to the reference one.

Devices	Reference Device	Developed Device
Quantum efficiency (%)	20	80
Base width (μm)	400	200
Reflectivity (%)	29	9

5. Conclusions

The effect of front surface recombination velocities and base thickness in solar cells' quantum efficiency were theoretically calculated. The results denote that both the surface recombination velocities and the base widths significantly impact the quantum efficiency. A good agreement was obtained between the experimental solar cells' quantum efficiency data and the theoretical results. Accordingly, the quantum efficiency of the mc-Si solar cells with porous silicon and rear interdigitated contact was enhanced up to 25% at a long wavelength range and up to 50% at a short wavelength compared to reference mc-Si solar cells. The obtained results indicate that the rear interdigitated contact reduced the base thickness and improved the charge carrier collection via larger contact rear areas, while the PS layer reduced the reflectance and diminished the front surface recombination velocities via the hydrogen-rich PS layer front surface passivation validated by the presence of Si-H bands. These results are of universal technical importance in designing solar cells and their surface structures. Overall, silicon solar cells with front-thin porous silicon and rear interdigitated contact have several perspectives (low cost, stability, and good efficiency) that make them an attractive option for developing efficient and cost-effective solar cells. With further research and development, these cells have the potential to play a significant role in the transition to a more sustainable and renewable energy future.

Author Contributions: All authors contributed to the study conception and design. Material preparation, data collection, and analysis were performed by B.A., L.K., A.G., A.A.A. and M.B.R. formal analysis by L.K., A.G. and A.A.A. The first draft of the manuscript was written by M.B.R. and B.A., data curation by B.A. and L.K., and supervision, M.B.R. All authors commented on previous versions of the manuscript. All authors have read and agreed to the published version of the manuscript.

Funding: This research received no external funding.

Institutional Review Board Statement: Not applicable.

Informed Consent Statement: Not applicable.

Data Availability Statement: Not applicable.

Acknowledgments: The authors extend their appreciation to the Deanship of Scientific Research at Imam Mohammad Ibn Saud Islamic University (IMSIU) for funding and supporting this work through the Research Partnership Program no RP-21-09-66.

Conflicts of Interest: The authors declare no conflict of interest.

References

1. Silicon Solar Cell Parameters. Available online: https://www.pveducation.org/pvcdrom/design-of-silicon-cells/silicon-solar-cell-parameters (accessed on 13 July 2022).
2. Surface Recombination. Available online: https://www.pveducation.org/pvcdrom/pn-junctions/surface-recombination (accessed on 13 July 2022).
3. Moshaev, V.; Leibin, Y.; Malka, D. Optimizations of Si PIN diode phase-shifter for controlling MZM quadrature bias point using SOI rib waveguide technology. *Opt. Laser Technol.* **2021**, *138*, 106844. [CrossRef]
4. Menahem, J.; Malka, D. A Two-Channel Silicon Nitride Multimode Interference Coupler with Low Back Reflection. *Appl. Sci.* **2022**, *12*, 11812. [CrossRef]
5. Faltakh, H.; Bourguiga, R.; Rabha, M.B.; Bessais, B. Simulation and optimization of the performance of multicrystalline silicon solar cell using porous silicon antireflection coating layer. *Superlattices Microstruct.* **2014**, *72*, 283–295. [CrossRef]
6. Joubert, P.; Guendouz, M.; Pedrono, N.; Charrier, J. Porous silicon micromachining to position optical fibres in silicon integrated optical circuits. *J. Porous Mater.* **2000**, *7*, 227. [CrossRef]

7. Rabha, M.; Khezami, L.; Jemai, A.; Alhathlool, R.; Ajbar, A. Surface passivation of silicon nanowires based metal nano-particle assisted chemical etching for photovoltaic applications. *J. Cryst. Growth* **2017**, *462*, 35–40. [CrossRef]
8. Khezami, L.; Al Megbel, A.O.; Jemai, A.B.; Rabha, M.B. Theoretical and experimental analysis on effect of porous silicon surface treatment in multicrystalline silicon solar cells. *Appl. Surf. Sci.* **2015**, *353*, 106–111. [CrossRef]
9. Yumen, Z.; Zhongming, L.; Chundong, M.; Shaoqi, H.; Zhimming, L.; Yuan, Y.; Zhiyun, C. Buried-contact high efficiency silicon solar cell with mechanical grooving. *Sol. Energy Mater. Sol. Cells* **1997**, *48*, 167.
10. Ebong, A.; Yun, F.; Ghozati, S.; Tang, Y.; Taouk, M.; Honsberg, C.; Wenham, S. Overcoming the open circuit voltage limit of the buried contact silicon solar cells. In Proceedings of the 12th European Photovoltaic Solar Energy Conference, Amsterdam, The Netherlands, 11–15 April 1994; pp. 1775–1777.
11. Ameer-Beg, S.; Perrie, W.; Rathbone, S.; Wright, J.; Weaver, W.; Champoux, H. Femtosecond laser micro structuring of materials. *Appl. Surf. Sci.* **1998**, *875*, 127–129.
12. Khezami, L.; Jemai, A.B.; Alhathlool, R.; Ben Rabha, M. Electronic quality improvement of crystalline silicon by stain etching-based PS nanostructures for solar cells application. *Sol. Energy* **2016**, *129*, 38–44. [CrossRef]
13. Kato, S.; Kurokawa, Y.; Soga, T. Enhancement of reflectance reduction of solar cells by a silicon nanoparticle layer on a textured silicon substrate. *Results Opt.* **2022**, *9*, 100296. [CrossRef]
14. Xu, J.; Chen, C.; Liu, C.; Chen, J.; Liu, Z.; Yuan, X.; Li, H. High efficiency TOPCon solar cells with micron/nano-structured emitter for a balance of light-trapping and surface passivation. *Sol. Energy Mater. Sol. Cells* **2022**, *238*, 111606. [CrossRef]
15. Ben Rabha, M.; Mohamed, S.B.; Dimassi, W.; Gaidi, M.; Ezzaouia, H.; Bessais, B. Optoelectronic enhancement of monocrystalline silicon solar cells by porous silicon-assisted mechanical grooving. *Physica Status Solidi C* **2011**, *8*, 887–890. [CrossRef]
16. Yang, W.J.; Ma, Z.Q.; Tang, X.; Feng, C.B.; Zhao, W.G.; Shi, P.P. Internal quantum efficiency for solar cells. *Sol. Energy* **2008**, *82*, 106–110. [CrossRef]
17. Brendel, R.; Hirsch, M.; Plieninger, R.; Werner, J.H. Quantum efficiency analysis of thin-layer silicon solar cells with back surface fields and optical confinement. *IEEE Trans. Electron Devices* **1996**, *43*, 1104–1112. [CrossRef]
18. Sze, S.M. *Physics of Semiconductor Devices*; Wiley & Sons: New York, NY, USA, 1981.
19. Kuo-Hui, Y.; Jaw-Yen, Y. The analysis of light trapping and internal quantum efficiency of a solar cell with DBR back reflector. *Sol. Energy* **2009**, *83*, 2050–2058.
20. Wolf, M.; Prince, M.B. New Developments in Silicon Photovoltaic Devices and Their Application in Electronics. *Proc. IEEE* **1958**, *18*, 583–595.
21. Saadoun, M.; Bessaïs, B.; Mliki, N.; Ferid, M.; Ezzaouia, H.; Bennaceur, R. Formation of luminescent $(NH\ 4)_2\ SiF_6$ phase from vapour etching-based porous silicon. *Appl. Surf. Sci.* **2003**, *210*, 88. [CrossRef]
22. Ben Rabha, M.; Bessaïs, B. Enhancement of photovoltaic properties of multicrystalline silicon solar cells by combination of buried metallic contacts and thin porous silicon. *Sol. Energy* **2010**, *84*, 486–491. [CrossRef]
23. Saadoun, M.; Mliki, N.; Kaabi, H.; Daoudi, K.; Bessais, B.; Ezzaouia, H.; Bennaceur, R. Vapour-etching-based porous silicon: A new approach. *Thin Solid Film.* **2002**, *405*, 29. [CrossRef]
24. Dimassi, W.; Bouaicha, M.; Saadoun, M.; Bessais, B.; Ezzaouia, H.; Bennaceur, R. Porous silicon-based passivation and gettering in polycrystalline silicon solar cells. *Nucl. Instrum. Meth. Phys. Res. B* **2002**, *186*, 441. [CrossRef]
25. Cho, Y.H.; Ebong, A.U.; Cho, E.C.; Kim, D.S.; Lee, S.H. Advanced buried contact solar cell structure. *Sol. Energy Mater. Sol. Cells* **1997**, *48*, 173. [CrossRef]
26. Kopitkovas, G.; Mikulskas, I.; Grigoras, K.; Simkiene, I.; Tomasiunas, R. Solar cells with porous silicon: Modification of surface-recombination velocity. *Appl. Phys. A Mater. Sci. Process* **2001**, *73*, 495–501. [CrossRef]
27. Krotkus, A.; Grigoras, K.; Paebutas, V.; Barsony, I.; Vazsonyi, E.; Fried, M.; Szlufcik, J.; Nijs, J.; Lévy-Clément, C. Efficiency improvement by porous silicon coating of multicrystalline solar cells. *Sol. Energy Mater. Sol. Cells* **1997**, *45*, 267–273. [CrossRef]
28. Nouri, H.; Bouacha, M.; Bessais, B. Effect of porous silicon on the performances of silicon solar cells during the porous silicon-based gettering procedure. *Sol. Energy Mater. Sol. Cells* **2009**, *93*, 1823–1826. [CrossRef]
29. Muduli, S.P.; Kale, P. State-of-the-art passivation strategies of c-Si for photovoltaic applications: A review. *Mater. Sci. Semicond. Proc.* **2023**, *154*, 107202. [CrossRef]
30. Lingaraja, D.; Kumar, S.P.; Ram, G.D.; Ramya, S. Experimental Investigation of Influence of Electrolytic Solution in Porous Silicon Formation for Solar Energy Conversion. *Silicon* **2023**, 1–8. [CrossRef]
31. Zhou, J.; Su, X.; Huang, Q.; Zhang, B.; Yang, J.; Zhao, Y.; Hou, G. Recent advancements in Poly-Si/SiOx passivating contacts for high-efficiency silicon solar cells: Technology review and perspectives. *J. Mater. Chem. A* **2022**, *10*, 20147–20173. [CrossRef]